Chaotic Dynamics for a Symmetry-Breaking Perturbation of the NLS Equation.

A. Calini
Department of Mathematics,
College of Charleston, Charleston, SC 29424
e-mail: calinia@cofc.edu

C.M. Schober
Department of Mathematics and Statistics,
Old Dominion University, Norfolk, VA 23529.
e-mail: cschober@lions.odu.edu

Abstract

For certain parameter regimes, the periodic focusing nonlinear Schrödinger equation (NLS) exhibits, under perturbation, a chaotic response characterized by irregular center-wing flipping of the wave form, when even spatial symmetry is imposed. The main source of chaos can be proven to be the transversal intersection of homoclinic manifolds of perturbed hyperbolic solutions. We study a symmetry breaking perturbation of the NLS equation, and observe novel types of chaotic behavior, including solutions which exhibit random flipping between a left and right modulated traveling wave. For the noneven case, we give a heuristic interpretation of these new phenomena in terms of Mel'nikov integrals.

1 Introduction.

The nonlinear Schrödinger equation (NLS) arises as the leading order approximation of nonlinear phenomena in numerous applications. The following generalization of the well known damped-driven perturbation of the focusing NLS equation (PNLS)

$$-iq_t + q_{xx} + 2|q|^2 q = \epsilon \left[i\alpha\, q + \Gamma e^{-2ic^2t+i\gamma} \left(1 - \delta \cos(2kx + x_0)\right)\right], \tag{1}$$

under periodic boundary conditions $q(x,t) = q(x+L,t)$, is of interest as the perturbation includes a spatially dependent term which breaks the symmetry with respect to space translation. When the parameter δ is zero and the potential is restricted to be even, i.e. $q(x,t) = q(-x,t)$, equation (1) exhibits a temporally chaotic evolution for a wide range of the parameters α and Γ. In this case successful analytical arguments have been found to explain the onset of chaotic dynamics as well as the spatial structure of the associated wave form. Persistence of hyperbolic solutions and transversal intersections of their homoclinic manifolds [7], and persistence of multi-jump homoclinic orbits [9] have been proven using singular perturbation theory and Mel'nikov analysis adapted to the infinite-dimensional setting.

However, in physical applications, evenness frequently does not have any physical justification. In the more general case when evenness is removed, very little is known theoretically. The evolution of asymmetric initial conditions has been studied numerically for a Hamiltonian perturbation of the NLS equation arising from a numerical discretization scheme [2, 6], and for a perturbation of the NLS equation coming from water wave experiments [8]. In the simplest noneven case, a train of modulated traveling wave solutions develops which randomly switches between left and right-traveling.

In this paper we study numerically and analytically the response of modulated periodic wavetrains to the PNLS equation in the noneven regime and initiate a Mel'nikov analysis to explain the onset of chaotic dynamics. We use initial conditions for which the discrete symmetry $x \to -x + x_0$ is not imposed, and we examine the effects of both continuous ($\delta \neq 0$) and discrete symmetry-breaking. In the numerical experiments, we choose initial conditions for finite-phase solutions close to a modulationally unstable plane wave with a single unstable mode. An extensive numerical study in which the initial data and the parameters α, δ and Γ have been varied provides some interesting results. Firstly, the onset of chaotic dynamics appears to be independent of the parameter δ, and the conditions on α and Γ to achieve the chaotic regime are the same in both the even and the non-even case. Secondly, for α and Γ satisfying the condition for chaos in the even case, when the parameter δ is turned on, we observe a combination of two phenomena: center-wing jumping about a shifted lattice site for certain time intervals and the occurrence of modulated traveling wave solutions randomly switching in time between left and right traveling. This type of mixed dynamics is sustained for very long times (T = 5000) and appears to be low-dimensional.

The low-dimensional character of the perturbed dynamics suggests a Mel'nikov type-approach to explain the chaotic evolution in terms of a transversal intersection of the homoclinic manifolds of persisting hyperbolic sets. When the even symmetry is removed, we view the space of finite-phase solutions close to a plane wave potential with one unstable mode as a six-dimensional phase space, containing a two-dimensional hyperbolic set and its four-dimensional degenerate homoclinic manifold. The two measurements needed to establish a transversal intersection of the perturbed stable and unstable manifolds can be computed explicitly in terms of the real and imaginary parts of the gradient of the Floquet discriminant functional.

Interestingly, we find that the resulting Mel'nikov integrals are computed to be, respectively, the time variation of the Hamiltonian and of the Linear Momentum functionals for the unperturbed equation along the unperturbed homoclinic orbit. The former is the well-known Mel'nikov integral which determines the conditions for chaotic dynamics in the even case.

Our numerical observations are consistent with the results of the heuristic Mel'nikov analysis. In the even regime (when δ is equal to zero), the Mel'nikov integral associated with the Linear Momentum functional is identically zero, and the threshold for the chaotic regime is given solely in terms of α and Γ as in previous studies. In this case only center-wing jumping without any spatial effects is observed.

In the noneven regime, the Mel'nikov integral associated with the Linear Momentum has a nondegenerate zero for any value of α and Γ, agreeing with the numerical observation that the onset of chaos is independent of δ and depends only on the parameters α and Γ. In this case, spatially irregular structures characterized by left-right switching between modulated traveling wave solutions are observed if the condition specified by the first Mel'nikov measurement is satisfied.

We begin this article with a brief review of the integrable theory for the NLS equation, and the use of Bäcklund transformations for constructing homoclinic solutions. Section 3 contains a heuristic description of the phase space geometry and a derivation of the Mel'nikov-type measurements by means of the Floquet discriminant functional. Finally, in Section 4 we describe the results of the numerical experiments including the spectral diagnostics which are summarized in the appendix.

2 Integrable Theory of the NLS.

Setting $\epsilon = 0$ in (1), we obtain the focusing cubic NLS equation which can be written in Hamiltonian form

$$i\partial_t \begin{pmatrix} q \\ \bar{q} \end{pmatrix} = J \begin{pmatrix} \delta H/\delta q \\ \delta H/\delta \bar{q} \end{pmatrix}, \tag{2}$$

with $J = \begin{pmatrix} 0 & 1 \\ -1 & 0 \end{pmatrix}$, and Hamiltonian

$$H(q, \bar{q}) = \int_0^L \left(|q_x|^2 - |q|^4 + 2\omega^2 |q|^2 \right) \, dx. \tag{3}$$

Zakharov and Shabat [1] established the complete integrability of the NLS equation by discovering its Lax pair:

$$\begin{aligned} \phi_x &= \mathcal{L}^{(x)} \phi \\ \phi_t &= \mathcal{L}^{(t)} \phi \end{aligned} \tag{4}$$

where

$$\mathcal{L}^{(x)} = \begin{pmatrix} i\lambda & iq \\ i\bar{q} & -i\lambda \end{pmatrix}, \qquad \mathcal{L}^{(t)} = \begin{pmatrix} i[2\lambda^2 - (q\bar{q} - \omega^2)] & 2i\lambda q + q_x \\ 2i\lambda\bar{q} - \bar{q}_x & -i[2\lambda^2 - (q\bar{q} - \omega^2)] \end{pmatrix} \tag{5}$$

The compatibility condition for the pair of linear systems (5) is satisfied for all values of the complex spectral parameter λ if the coefficient $q(x,t)$ satisfies the NLS equation (1) at $\epsilon = 0$. If one imposes periodicity by requiring the potential $q(x,t)$ to be periodic in the spatial variable x with period L, then one can characterize q (for any fixed time t) in terms of its Floquet spectrum

$$\sigma(\mathcal{L}^{(x)}(q)) := \left\{ \lambda \in \mathbb{C} \mid \mathcal{L}^{(x)}\boldsymbol{v} = 0, |\boldsymbol{v}| \text{ bounded } \forall x \right\}. \tag{6}$$

Given a fundamental solution matrix $M(x;\lambda)$ (such that $M(0;\lambda) = I$) for the Lax pair (4) with potential $q(x)$, one defines the the Floquet discriminant to be the trace of the transfer matrix $M(L;\lambda)$ across one period:

$$\Delta(q;\lambda) := \mathrm{Tr}[M(L;\lambda)]. \tag{7}$$

Since $\det[M(x;\lambda)] = 1$, the Floquet spectrum can be characterized as follows:

$$\sigma(\mathcal{L}^{(x)}(q)) := \{ \lambda \in \mathbb{C} \mid \Delta(q;\lambda) \text{ is real and } -2 \le \Delta(q;\lambda) \le 2 \}. \tag{8}$$

Within the discrete spectrum, periodic/antiperiodic eigenvalues are the roots of $\Delta(q;\lambda) = \pm 2$. We also distinguish

$$\begin{array}{ll} \text{critical points} & \left\{ \lambda \in \mathbb{C} \;\middle|\; \dfrac{d\Delta}{d\lambda} = 0 \right\}, \text{ and} \\ \text{multiple points} & \{ \lambda \in \mathbb{C} \mid \lambda \text{ critical}, \ \Delta = \pm 2 \}. \end{array}$$

Generic multiple points have multiplicity two; complex double points are in general associated with critical saddle-like level sets and can be used to label their homoclinic orbits.

We summarize the properties of the Floquet discriminant which will be used in the following sections:

(a) $\Delta(q;\lambda)$ is constant under the NLS evolution.

(b) Floquet discriminants at different values of the spectral parameter Poisson commute: for $\lambda \neq \lambda'$,

$$\{\Delta(q;\lambda), \Delta(q;\lambda')\},$$

where the Poisson bracket is defined as

$$\{F, G\} = i \int_0^L \left(\frac{\delta F}{\delta q} \frac{\delta G}{\delta \bar{q}} - \frac{\delta F}{\delta \bar{q}} \frac{\delta G}{\delta q} \right) dx.$$

(c) $\Delta(q, \bar{q}, \lambda)$ is an analytic function of its arguments. The first variation [4] with respect to q and $\bar{q}$ is given by

$$\delta\Delta(q, \bar{q}; \lambda) = \int_0^L \left[\frac{\delta\Delta}{\delta q} \, \delta q(x) + \frac{\delta\Delta}{\delta \bar{q}} \, \delta\bar{q}(x) \right] dx,$$

where

$$\begin{aligned} \frac{\delta\Delta(q,\bar{q};\lambda)}{\delta q} &= -\frac{i}{2} \,\mathrm{Tr}\left[M^{-1}(x) \begin{pmatrix} 0 & 1 \\ 0 & 0 \end{pmatrix} M(x+L) \right] \\ \frac{\delta\Delta(q,\bar{q};\lambda)}{\delta \bar{q}} &= -\frac{i}{2} \,\mathrm{Tr}\left[M^{-1}(x) \begin{pmatrix} 0 & 0 \\ 1 & 0 \end{pmatrix} M(x+L) \right]. \end{aligned} \tag{9}$$

Properties (a) and (b) show how $\Delta(q;\lambda)$ encodes the infinite family of NLS constants of motion (in fact, parametrized by $\lambda \in \mathbb{C}$).

2.1 Homoclinic orbits.

A complete analytical description of the stable and unstable manifolds of critical level sets of unstable finite-gap NLS potentials is available in terms of exact formulae for their homoclinic orbits. Although perhaps the most direct construction of homoclinic solutions comes from formulae for dark solitons, we derive them using Bäcklund transformations built from squared eigenfunctions for the associated potential. In this way, we obtain a parametrization of the homoclinic solutions which has a direct geometrical interpretation.

One starts with the general solution of $\vec{\phi} = c_+\vec{\psi}^+ + c_-\vec{\psi}^-$ of the Lax pair (4) evaluated at a complex double point $\lambda = \lambda_d$ of the spectrum of an unstable solution $q(x)$, where $\vec{\psi}^\pm$ are the associated Bloch eigenfunctions. The following matrix defines a gauge transformation from the eigenfunction $\psi^\pm(\lambda)$ corresponding to the "seed solution" $q(x)$ to the eigenfunction $\Psi^\pm(\lambda)$ associated with the new potential $q^H(x)$:

$$G(\lambda) = N \begin{pmatrix} \lambda - \lambda_d & 0 \\ 0 & \lambda - \bar{\lambda}_d \end{pmatrix} N^{-1}, \qquad N = \begin{pmatrix} \phi_1 & -\bar{\phi}_2 \\ \phi_2 & \bar{\phi}_1 \end{pmatrix}. \tag{10}$$

The eigenfunctions $\Psi^\pm(\lambda)$ and potential $q^H(x)$ are given by

$$q^H = q + 2(\lambda_1 - \bar{\lambda}_1)\frac{\phi_1\bar{\phi}_2}{|\phi_1|^2 + |\phi_2|^2}, \qquad \Psi^\pm(\lambda) = G(\lambda)\psi^\pm(\lambda), \tag{11}$$

and satisfy the following properties:

(i) The eigenfunction $\Psi^\pm(\lambda)$ solves the Lax pair (4) at (q^H, λ).

(ii) $\sigma(\mathcal{L}^{(x)}(q^H)) = \sigma(\mathcal{L}^{(x)}(q))$, that is, the Bäcklund transformation is isospectral.

(iii) $q^H(x+L) = q^H(x)$ is an NLS solution homoclinic to $q(x,t)$, i.e.

$$\lim_{t\to\pm\infty} q^H(x,t) = e^{i\gamma^\pm} q(x,t),$$

where the limit is approached exponentially at a rate depending on the complex double point λ_d.

For a plane wave solution $q(x,t) = ae^{2ia^2t}$, the corresponding Floquet discriminant is readily computed to be

$$\Delta(a,\lambda) = 2\cos(\sqrt{a^2+\lambda^2}L). \tag{12}$$

Then, the associated Floquet spectrum consists of continuous bands $\mathbb{R}\bigcup[-ia, ia]$, and a discrete part containing the simple periodic/antiperiodic eigenvalues $\pm i|a|$, and the infinite number of double points

$$\lambda_n^2 = \left(\frac{n\pi}{L}\right)^2 - a^2, \qquad n \in \mathbb{Z}. \tag{13}$$

Of these, if $[aL/\pi] = M$ (where $[p] =$ largest integer $\leq p$, $p > 0$), $2M$ are complex (pure imaginary) double points, while the remaining λ_n's for $|n| > M$, are real double points. In the numerical experiments we use initial conditions which are small finite-genus perturbations of unstable plane waves with one unstable mode (the "one-complex double point regime"); this is the case, provided $[aL/\pi] = 1$.

The homoclinic orbit of the plane wave solution can be constructed using the method described above. The pair of imaginary double points is $\lambda_d^\pm = \pm i\sqrt{a^2 - (\pi/L)^2}$, and the corresponding Bloch eigenfunctions are

$$\psi^\pm = \frac{i}{2}ke^{\mp i(\pi/4 - p/2)} \begin{pmatrix} ae^{-i(2a^2t+\gamma)/2} \\ \pm ae^{\mp ip}e^{i(2a^2t+\gamma)/2} \end{pmatrix} e^{\pm ik(x+2\lambda t)}, \tag{14}$$

where we introduce the parameters $k = \sqrt{a^2+\lambda_1^2}$ and $k(\lambda_d^+) + \lambda_d^+ = ae^{ip}$. Setting $\sigma = -2i\lambda_d^+k(\lambda_d^+)$ and $c_+/c_- = e^{\rho+i\beta}$, we obtain the following expression for the homoclinic orbit

$$q^H(x,t;\lambda_d^+) = ae^{-i(2a^2t+\gamma)}\frac{\cos 2p\cosh(\sigma t - \rho) - i\sin 2p\sinh(\sigma t - \rho) - \sin p\cos(2kx+\beta)}{\cosh(\sigma t - \rho) + \sin p\cos(2kx+\beta)}. \tag{15}$$

If one requires the homoclinic orbit to have the even symmetry $q^H(-x) = q^H(x)$, then the angle β must be selected to be 0 or π, giving a pair of disconnected homoclinic orbits. However, without the even constraints, the homoclinic manifold of the plane wave solution is connected, as we will discuss in the next section.

3 Geometry and Mel'nikov Analysis.

3.1 Dimension counting in the relevant phase space.

We give a heuristic description of the geometry of a neighborhood of a modulationally unstable plane wave with one unstable mode, consisting of finite-phase solutions whose Floquet spectra are "close" to the one of the unstable plane wave. In Figure 1 we show the spectral configuration of one of these solutions.

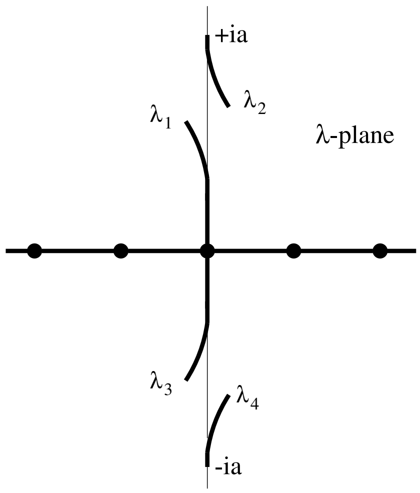

Figure 1: The Floquet spectrum of a three-phase solution close to an unstable plane wave in the one-complex double point regime.

In [3] the isospectral set of a noneven three-phase solution is shown to be diffeomorphic to a three-dimensional torus $S^1 \times S^1 \times S^1$ (each S^1 corresponding to the angle variable for a μ-cycle on the associated Riemann surface). It follows that the neighborhood Π of three-phase solutions of the plane wave potential in the one-complex double point regime is six dimensional.

In the critical case, for which $\lambda_1 = \lambda_2$ and $\lambda_3 = \lambda_4$, the corresponding homoclinic manifold of the plane wave solution $q(x) = a$ (we are setting $t = 0$) is diffeomorphic to the disjoint union $S^1 \cup S^1 \times (S^1 \times \mathbb{R})$. In expression (15) of the homoclinic orbit, the parameters (γ, β, ρ) can be interpreted as the coordinates of $S^1 \times (S^1 \times \mathbb{R})$ (the first one parametrizes the target solution, the second is the phase labeling the family of homoclinic orbits, while ρ is a parameter, or initial time between $-\infty$ and $+\infty$, along each homoclinic orbit).

Since the one-complex double point regime is obtained for an open interval $\mathcal{A}$ of values of the amplitude a for which $[aL/\pi] = 1$, then, within the invariant six-dimensional neighborhood Π, one has a two-dimensional hyperbolic manifold $q_a = ae^{i\gamma}$ (parametrized by $a \in \mathcal{A}$ and $\gamma \in S^1$), with four-dimensional stable and unstable manifold q^H parametrized by $(a, \gamma, \beta, \rho) \in \mathcal{A} \times S^1 \times S^1 \times \mathbb{R}$ as in formula (15).

If even spatial symmetry is not imposed, the parameter β is free to take any value in S^1. As a consequence, the stable and unstable manifold q^H is connected (unlike for the even case in which it has two connected components, one for $\beta = 0$ and one for $\beta = \pi$, corresponding to a pair of distinct homoclinic orbits in formula (15)).

Under a perturbation which preserves the six-dimensional subspace of three-phase solutions, as is the case treated in this work, the four-dimensional invariant manifolds generically split and may intersect transversally along a two dimensional hyperbolic manifold q_a^ϵ (an x-dependent perturbation of the hyperbolic family of plane wave solutions q_a). Therefore, in order to construct a Mel'nikov measurement to establish a transversal intersection of the stable and unstable manifolds, we need to measure the splitting along two independent directions transversal to the unperturbed invariant manifold q_H. Next, we discuss how the gradient of the Floquet discriminant provides appropriate transversal directions to the unperturbed invariant manifold.

3.2 Fundamental Invariants.

The Floquet discriminant implicitly defines the unperturbed homoclinic manifold as

$$\Delta(q^H, \lambda^c) = -2. \tag{16}$$

For unstable potentials with a low number of unstable modes, the Floquet discriminant functional has been shown to provide a More function-type approach to the study of the topology of the critical level sets, labeled in terms of the complex double points for the gievn potential [5].

Given a potential q_0 with a complex critical eigenvalue λ^c, let $\mathcal{N}_b = \mathcal{N}_b(q_0)$ be a neighborhood of q_0. Regarding the critical point as a functional on $\mathcal{N}$, $\lambda^c = \lambda^c(q)$, we have

$$\frac{\partial}{\partial \lambda}\Delta(\lambda; q)\bigg|_{\lambda^c(q)} = 0, \qquad\qquad \lambda^c(q_0) = \lambda^c.$$

We introduce the invariant functional:

$$F : \mathcal{N}_b \to \mathbb{R} \qquad\qquad F := \Delta(\lambda^c(q); q). \tag{17}$$

F is a smooth function of q, provided $\frac{d^2\Delta(\lambda,q)}{d\lambda^2} \neq 0,\ \forall\, q \in N_b$. As in [5], we define the following natural sequence of constants of motion

$$F_j(q) = \Delta(\lambda_j^c(q), q),$$

generated as λ_j^c varies among the critical points for the potential q. The invariants F_j's can be used to provide a local description of the strata which are close to critical level sets of saddle type. Such a local analysis is encoded in the first and second variation of the F_j's. The gradient of F_j has a simple explicit representation in terms of the Bloch eigenfunctions (see [5]). Let $\vec{\psi}^{\pm}(x, \lambda)$ denote the Bloch eigenfunctions of the the Lax pair (5) at $(q; \lambda)$; these are common eigenfunctions of the linear operator $\mathcal{L}^{(x)}(q; \lambda)$ and the shift operator $x \to x + L$, and are defined (up to normalization) by

$$\vec{\psi}(x + L, \lambda) = \rho(\lambda)\vec{\psi}(x, \lambda). \tag{18}$$

Here $\rho(\lambda)$ denotes the Floquet multiplier, related to the Floquet discriminant by

$$\rho(\lambda) = \frac{1}{2}\left[\Delta(\lambda) + \sqrt{\Delta^2(\lambda) - 4}\right]. \tag{19}$$

One computes the functional gradients of the F_j's with respect to $\vec{q} = (q, \bar{q})$ to be

$$\frac{\delta F_j}{\delta \vec{q}}(q) = i\frac{\sqrt{\Delta^2 - 4}}{W[\psi^+, \psi^-]}\begin{bmatrix} \psi_2^+\psi_2^- \\ -\psi_1^+\psi_1^- \end{bmatrix}\Bigg|_{\lambda=\lambda^c}, \tag{20}$$

where $W[\psi^+, \psi^-]$ denotes the Wronskian of ψ^+ and ψ^-. One can verify that $\dfrac{\delta F_j}{\delta \vec{q}}(q_0) = 0$, that is , the functional F_j is critical at the critical level set. If q^H is a homoclinic orbit in the isospectral level set of q_0, then its associated Bloch eigenfunctiosn $\Psi^{\pm}$ can be explicitly constructed using Bäcklund transformations as in (11). The corresponding gradient

$$\frac{\delta F_j}{\delta \vec{q}}(q^H) = i\frac{\sqrt{\Delta^2 - 4}}{W[\Psi^+, \Psi^-]}\begin{bmatrix} \Psi_2^+\Psi_2^- \\ -\Psi_1^+\Psi_1^- \end{bmatrix}\Bigg|_{\lambda=\lambda^c} \tag{21}$$

does not vanish. Therefore $\delta F_j/\delta\vec{q}(q^H)\big|_{\lambda^c}$ defines a direction transversal to the homoclinic manifold and can be used to construct a Mel'nikov type measurement.

3.3 Mel'nikov integrals.

If we do not work in the space of even potentials, the Floquet discriminant $\Delta(\lambda)$ is in general a complex-valued functional. For the one-complex point regime, we denote with λ_1 the only complex double point of the plane wave solution of the unperturbed equation, and set $q = u + iv$ and $F_1(q_0) = \Delta(\lambda_1(q_0), q_0) = F_1^R + iF_1^I$. Then, the two directions transversal to the unperturbed homoclinic manifolds are given by the real-valued gradients

$$\left(\frac{\partial F_1^R}{\partial u}, \frac{\partial F_1^R}{\partial v}\right)\Big|_{q^H}, \qquad \left(\frac{\partial F_1^I}{\partial u}, \frac{\partial F_1^I}{\partial v}\right)\Big|_{q^H}.$$

Using formula (15) for the homoclinic orbit of the plane wave solution $q_a(t) = ae^{-2ia^2(t-t_0)}$, computing the expression of the associated Bloch eigenfunctions, and using the Bäcklund transformation (11), we can show that the gradients of the real and imaginary part of F_1 are proportional, respectively, to the gradients of the Hamiltonian and the Momentum functionals:

$$\begin{aligned} H[q] &= \int_0^L \left(q_x\bar{q}_x - q^2\bar{q}^2\right)\, dx = \int_0^L \left[(u_x)^2 + (v_x)^2 - (u^2+v^2)^2\right]\, dx \\ P[q] &= \frac{1}{2i}\int_0^L \left(q_x\bar{q} - q\bar{q}_x\right)\, dx = \int_0^L \left(u\, v_x - u_x\, v\right)\, dx \end{aligned} \tag{22}$$

We compute $\mathrm{grad}(F_1^R) \sim \mathrm{grad}(H) + 4a^2(u,v)$, and the corresponding Mel'nikov integral [1]

$$M_H = \int_{-\infty}^{\infty}\int_0^L \left(\frac{\partial F_1^R}{\partial u} f_u + \frac{\partial F_1^R}{\partial v} f_v\right)\Big|_{(u^H,v^H)} dx\, dt =$$

$$= \int_{-\infty}^{\infty} \frac{dH}{dt}\Big|_{q^H} dt - 4a^2 \int_{-\infty}^{\infty}\int_0^L \left(uf_u + vf_v\right)|_{(u^H,v^H)}\, dx\, dt.$$

The vector (f_u, f_v) is the vector of the perturbation, where $f_u = -\alpha u + \Gamma\sin(\phi)\cos(2kx + x_0)$ and $f_v = -\alpha v + \Gamma\sin(\phi)\cos(2kx + x_0)$ (ϕ is a constant phase depending on α, t_0 and γ).

We also compute $\mathrm{grad}(F_1^I) \sim \mathrm{grad}(P)$ and its associated Mel'nikov integral,

$$M_P = \int_{-\infty}^{\infty}\int_0^L \left(\frac{\partial F_1^I}{\partial u} f_u + \frac{\partial F_1^I}{\partial v} f_v\right)\Big|_{(u^H,v^H)} dx\, dt = \int_{-\infty}^{\infty} \frac{dP}{dt}\Big|_{q^H} dt.$$

Since the linear momentum is the generator of spatial translation, we expect the nondegenerate zeros of M_P to be related to the symmetry breaking patterns observed in the noneven chaotic regime.

The explicit parameter dependence of the two Mel'nikov integrals, is given below. Up to constant coefficients (independent of the relevant parameters), and having set $c^2 = a^2$, we compute

$$M_H = \epsilon\frac{\pi}{\sigma k}\cos^2 p\, (\alpha a + \Gamma\sin b)\, Y_H, \tag{23}$$

where $b = a\rho + \gamma$, and Y is the nonvanishing integral

$$Y_H = \int_{-\infty}^{\infty} \frac{\cosh\tau}{(\cosh^2\tau - \sin^2 p)^{\frac{3}{2}}}\, d\tau.$$

The condition for nondegenerate zeros of M_H is given in terms of a linear relation between the damping α and the driving amplitude Γ. Expression (23) and a rigorous analysis of the implications of its nondegenerate zeros can be found in [7]. We remark that M_H is independent of δ (this holds only when the forcing frequency c^2 is the same as the frequency a^2 of the plane wave solution, as required in the analysis).

As for the Mel'nikov integral associated with the linear momentum, we have

$$M_P = -\epsilon\delta\Gamma\frac{\pi}{\sigma k}\frac{\cos b}{\sin^2 p}\sin(x_0 - \beta)\, Y_P, \tag{24}$$

[1] The second term in its expression subtracts off the oscillatory term in the time derivative of the Hamiltonian, making the integral strongly convergent.

where

$$Y_P = \int_{-\infty}^{+\infty} \left(\frac{\cosh \tau}{\sqrt{\cosh^2 \tau - \sin^2 p}} - 1 \right) [\cosh \tau \cos(a\tau) \cos p + \sinh \tau \sin(a\tau) \sin p] \, d\tau.$$

We distinguish two cases:

(a) If $x_0 = \beta$, that is if the perturbation is "in phase" with the unperturbed homoclinic orbit, then the evolution takes place in the invariant subspace of solutions even with respect to the symmetry $x \to -x + \beta\pi/k$. This follows from the fact that, in this very low-dimensional case, the homoclinic orbit (15) possesses such a symmetry. Effectively, we are in the even regime. In this case, the second measurement is identically zero and the onset of chaotic behavior can be established by means of the first condition only.

(b) If $x_0 \neq \beta$, then spatial symmetry of the solutions is broken. Correspondingly, the Mel'nikov integral M_P possesses the nondegenerate zeros $b = \pi/2, 3\pi/2$. We expect then to observe non even effects in the chaotic wave form, whenever the condition for homoclinic chaos given by the first measurement M_H is met. This is indeed the case, as shown by the numerical experiments.

4 Numerical Experiments.

We examine the longtime dynamics of the PNLS equation (1) by choosing initial conditions in the vicinity of the homoclinic orbit q^H (15) of the following form,

$$\begin{aligned} q(x,0) &= q^H + \epsilon_1 q^H_\gamma + \epsilon_2 q^H_x \\ &= (1 - \epsilon_1 i) c e^{-i\gamma} \left(\frac{\cos 2p \cosh \rho + i \sin 2p \sinh \rho - \sin p \cos(2kx + \beta)}{\cosh \rho + \sin p \cos(2kx + \beta)} \right) \\ &\quad + \epsilon_2 c e^{-i\gamma} \left(\frac{(2k \sin p \sin(2kx + \beta))(\cosh \rho + \cos 2p \cosh \rho + i \sin 2p \sinh \rho)}{(\cosh \rho + \sin p \cos(2kx + \beta))^2} \right) \end{aligned} \tag{25}$$

where $L = 2\sqrt{2}$, parameters k, p, ρ are defined in section 2.1 and parameters c, γ, β are free to vary. The evolution of this initial data under the NLS equation is a waveform with a single coherent structure localized at either the center or edge of the period which recurs periodically in time. We numerically integrate the PNLS equation using an exponentially accurate (for analytic solutions) Fourier pseudospectral scheme in space and a fourth order Runge-Kutta discretization in time. The truncation errors are $\mathcal{O}(10^{-8})$, well below the strength of the perturbative terms, so the phenomena observed numerically cannot be attributed to truncation errors.

The Mel'nikov analysis indicates the possibility of observing a sustained chaos that appears on a short to moderate time scale for appropriate values of the perturbation parameters α and Γ. For fixed α, in both the even and noneven regimes, the route to chaos as the strength of the driver Γ is gradually increased is as follows: the solution is temporally dissipative, then periodic, then chaotic and finally locked to the driver. Varying the initial data or strength of α it is possible to obtain an additional transition in the bifurcation sequence, i.e. the solution is temporally dissipative, then periodic, then "sech" type, then chaotic and finally locked to the driver.

We examined the bifurcation sequence for various values of α, i.e. $\mathcal{O}(10^{-3})$ to $\mathcal{O}(10^{-1})$, in both the even and noneven case. The specific transition values of Γ in the bifurcation sequence vary slightly depending on the initial data, values of α used and whether $\delta = 0$ or not. However, the transition to chaotic dynamics in both the even and noneven regime always occurs for parameter values consistent with the lower bound provided by the Mel'nikov analysis, $\Gamma > \alpha/2$. Consequently, the onset of chaos does not appear to depend on δ. Figures 2-3 show typical chaotic solutions in the even and noneven regime, respectively, which demonstrate both the consistency of our numerical results with the Mel'nikov analysis and the distinguishing features of the chaotic waveform in these regimes.

The surface of the waveform obtained using (1) for initial data (25) with parameter values $\alpha = .05$, $\Gamma = .06$, $\delta = 0$, $x_0 = \beta = 0$ and $c = .5$ is given in Figure 2a for the time frame $100 < t < 200$. The Mel'nikov analysis indicates that this is data for the chaotic even regime as M_H has nondegenerate zeros and

$M_P \equiv 0$. For these parameter values, the solution obtained with the PNLS equation is temporally chaotic and is characterized by a random flipping in time in the wave form between the center and edge of the period (denoted center-wing flipping). The evolution of the spectrum is given in Figure 2b. The splitting function D_1 (see the appendix for the details on interpreting the spectral diagnostics) exhibits random homoclinic crossings and a flipping between cross and gap states, which is a reflection of the center-wing flipping in the waveform. This behavior is sustained on the time frame examined, $0 < t < 5000$. It is worth noting that although the solution is temporally chaotic, spatially the solution is localized at two distinct sites.

The behavior in the noneven chaotic regime is considerably more complex. Figure 3a shows the surface of the waveform shortly after the onset of irregular motions, $100 < t < 200$, obtained using (1) for initial data (25) with $\alpha = .15$, $\Gamma = .17$, $\delta = .5$, $x_0 = 1$, $\beta = 0$ and $c = .5$. In this case both of the Mel'nikov integrals M_H and M_P have nondegenerate zeros. Initially the waveform is spatially even, but, as time evolves, it loses symmetry due to the noneven perturbation. The waveform exhibits center-wing jumping about a shifted lattice site for certain time intervals and bifurcations across standing wave states between left and right traveling modulated waves for other time intervals. For example in Figure 3a transitions in the waveform between left and right traveling occur at about $t = 115$ and $t = 170$. This is confirmed by examining the evolution of the spectrum of the perturbed solution. Figure 3b. shows the evolution of $D(\lambda_+, \lambda_-)$, $V(\lambda_+, \lambda_-)$ and $H(\lambda_+, \lambda_-)$ (see the appendix for details) under the PNLS flow for $0 < t < 500$. From the evolution of the splitting distance $D(\lambda_+, \lambda_-)$ it is clear that homoclinic crossings do not occur. The vertical and horizontal splitting functions $V(\lambda_+, \lambda_-)$ and $H(\lambda_+, \lambda_-)$ have frequent random zeros indicating that the single complex double point splits asymmetrically and switches from the configuration of a right traveling to the configuration of a left traveling modulated two-phase solution, passing through gap and cross configurations. In particular $V(\lambda_+, \lambda_-)$ and $H(\lambda_+, \lambda_-)$ have zeros at $t = 115$ and $t = 170$. This type of irregular dynamics is sustained for very long times (T = 5000) and appears to be low-dimensional.

An important feature of the noneven regime is that in addition to temporally chaotic behavior, the solution appears to be spatially irregular. Throughout the time series, it is not known which spatial site the mode will be localized about. This suggests the possibility of spatial chaos in the sytem when $\delta \neq 0$. A statistical study of the spatial independence of the PNLS system would be interesting to pursue to investigate whether the loss of spatial symmetry has any relation with spatially chaotic waveforms.

It should be stressed that chaotic motions are obtained in the noneven regime only if M_H has nondegenerate zeros. When $M_H \neq 0$ (but M_P does have nondegenerate zeros), in longtime simulations we obtain a noneven solution which does not display temporally chaotic behavior; there is no chaotic switching between left and right traveling states. Consequently, nondegenerate zeros of M_P are a necessary but not sufficient condition for chaotic left-right switching. Once the condition for chaos (through M_H) is satisfied then if M_P is identically zero we obtain only center wing jumping whereas if M_P has nondegenerate zeros, the chaotic waveform has complicated spatial structure characterized by left-right switching.

Acknowledgements.

This work was partially supported by the NSF, grant number DMS-9705005 and DMS-9803567.

5 Appendix.

5.1 Nonlinear diagnostics.

The near-integrable dynamics of (1) can be interpreted in terms of the known dynamical properties of the NLS equation when we examine the evolution of the nonlinear spectrum of NLS under perturbation. At each time t, we take the numerically generated solution $\{q_n(t) | n = 1, \ldots, N\}$ and perform a direct spectral transform to numerically compute the Floquet spectrum $\sigma(\lambda)$ (defined in section 2). By monitoring the evolution of the spectrum, the behavior of the numerical solution can be correlated to changes in the type of solution in the neighborhood of the critical level set.

Under small perturbations each complex double point splits into two simple points $\lambda_\pm$, the type of splitting depending on whether the perturbation is even or noneven. For even initial data, when the double point splits $(\lambda_+ - \lambda_-)$ is either real or pure imaginary; i.e. the double point splits into either a "gap"

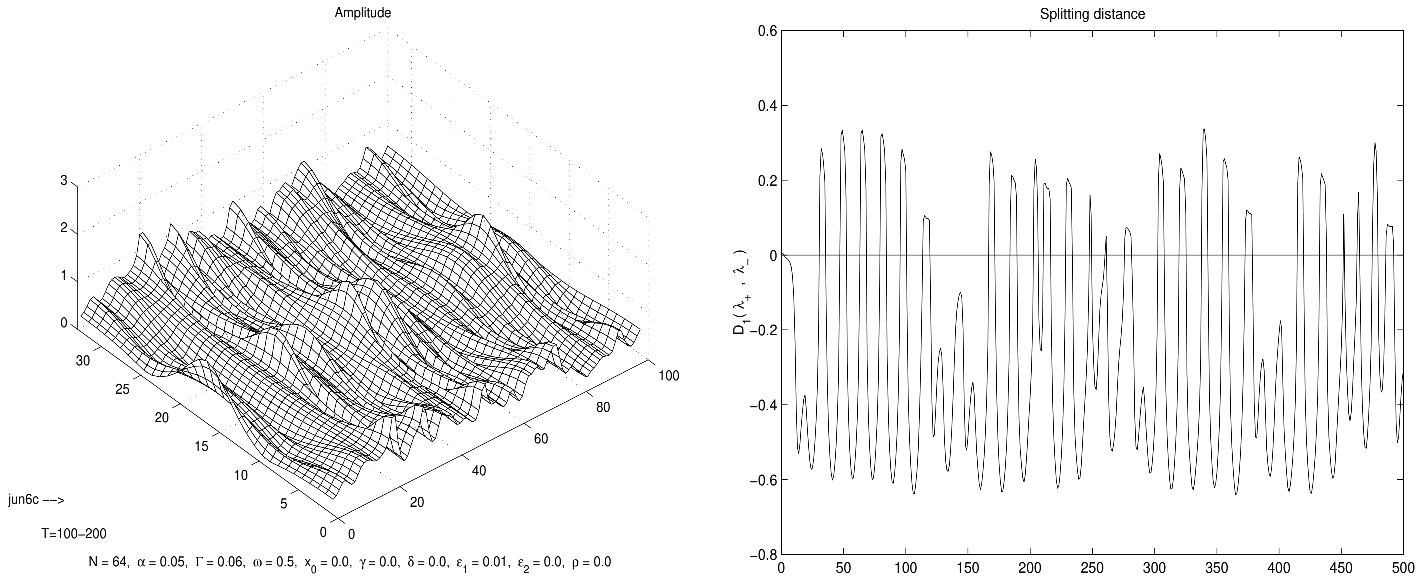

Figure 2: Temporal chaos in the even regime. a) Surface obtained with (1) for $100 < t < 200$. b) The evolution of $D_1(\lambda_+, \lambda_-)$ for the first mode for $0 < t < 500$. Homoclinic crossings occur at the zeros of D_1.

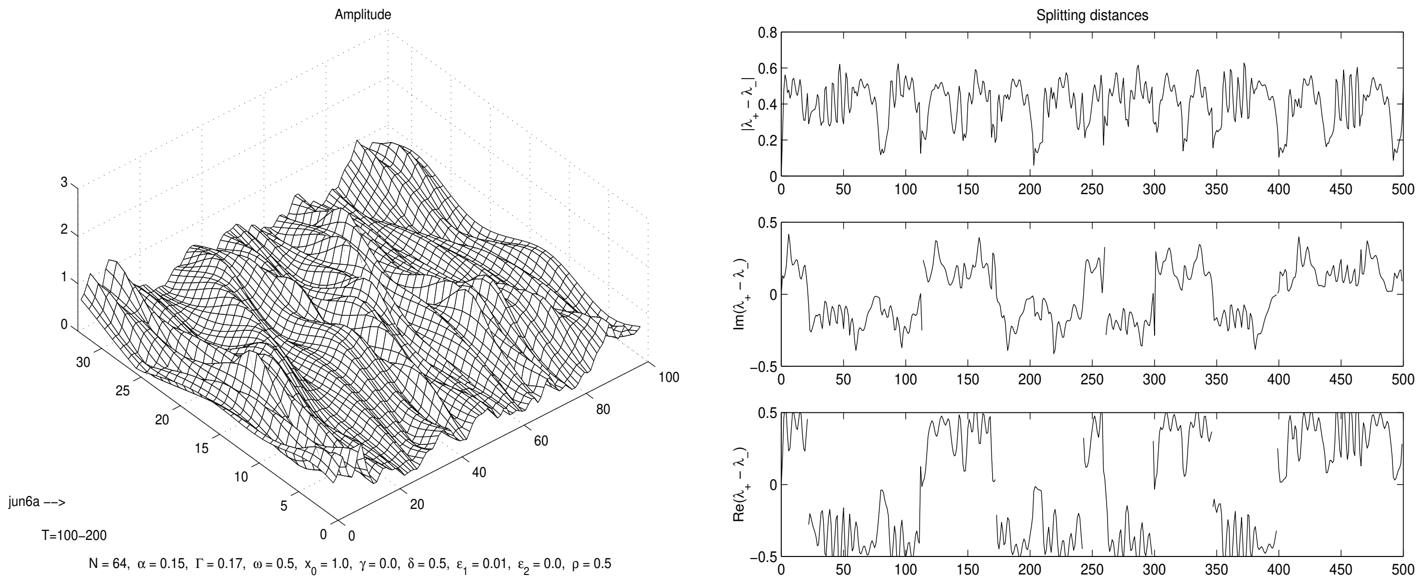

Figure 3: Temporal chaos in the noneven regime. Complicated spatial structure is also exhibited. a) Surface obtained with (1) for $100 < t < 200$. b) The evolution of $D(\lambda_+, \lambda_-)$, $V(\lambda_+, \lambda_-)$ and $H(\lambda_+, \lambda_-)$ for the first mode for $0 < t < 500$. Transitions between left and right going waves occur at the zeros of V and of H.

state along the imaginary axis or symmetrically about the imaginary axis into a "cross" state. In even experiments we monitor the evolution of the splitting distance $D(\lambda_+,\lambda_-) = |\lambda_+ - \lambda_-|$ in time, and present a signed measure of this splitting distance, i.e.

$$D_1(\lambda_+,\lambda_-) = \begin{cases} +|\lambda_+ - \lambda_-| & \text{if } Re(\lambda_+ - \lambda_-) = 0 \\ -|\lambda_+ - \lambda_-| & \text{if } Im(\lambda_+ - \lambda_-) = 0. \end{cases} \tag{26}$$

Positive and negative values represent gap and cross states respectively and a sign change represents a homoclinic crossing.

In the noneven case, $(\lambda_+ - \lambda_-)$ has, in general, both a real and an imaginary part. The spectral measurements relevant in experiments using noneven initial conditions are: the splitting distance $D(\lambda_+,\lambda_-)$ and the "vertical" and "horizontal" splitting, which we denote $V(\lambda_+,\lambda_-)$ and $H(\lambda_+,\lambda_-)$. The vertical splitting is a signed measure of the splitting distance $Im(\lambda_+ - \lambda_-)$, where we correlate the sign with left and right traveling wave states, i.e.

$$V(\lambda_+,\lambda_-) = \begin{cases} +Im(\lambda_+ - \lambda_-) & \text{if } Re\lambda_+ \geq 0 \\ -Im(\lambda_+ - \lambda_-) & \text{if } Re\lambda_+ < 0. \end{cases} \tag{27}$$

For $V > 0$ the wave is right going, for $V = 0$ the wave is standing and for $V < 0$ the wave is left going. Transitions between left and right traveling waves also occur when the spectrum changes configuration by evolving through a gap state. This can be detected by examining $Re(\lambda_+ - \lambda_-)$ and we monitor

$$H(\lambda_+,\lambda_-) = \begin{cases} +Re(\lambda_+ - \lambda_-) & \text{if } Re\lambda_+ \geq 0 \\ -Re(\lambda_+ - \lambda_-) & \text{if } Re\lambda_+ < 0. \end{cases} \tag{28}$$

For a homoclinic crossing or double point crossing to occur, λ_+ and λ_- must coalesce and $D(\lambda_+,\lambda_-) = 0$. For $D(\lambda_+,\lambda_-) \neq 0$, when the vertical or horizontal splitting passes through zero the spectral configuration evolves through a cross or gap state respectively and the waveform bifurcates across a standing wave solution into (either left or right going) traveling waves. In monitoring the spectrum, when either of the diagnostics V or H is zero then the solution evolves through a cross or gap state respectively. It crosses the level set of stationary solutions $M_P = 0$. In Figure 3b, the vertical splitting V is labeled $Im(\lambda_+ - \lambda_-)$ and the horizontal splitting H is labeled $Re(\lambda_+ - \lambda_-)$. These two plots should be interpreted together. When V has a zero there is a discontinuous jump in H and vice versa.

References

[1] V.E. Zakharov and A.B. Shabat, Exact theory of two-dimensional self-focusing and one-dimensional self-modulation of waves in nonlinear media. *Soviet Phys. Jetp* **34** (1972) 62–69.

[2] D.W. McLaughlin and C.M. Schober, Chaotic and homoclinic behavior for numerical discretizations of the nonlinear Schrödinger equation. *Physica D* **57** (1992) 447–465.

[3] N.M. Ercolani and D.W. McLaughlin, Toward a topological classification of integrable PDE's. MSRI Proc. Workshop on Symplectic Geometry. R. Devaney, H. Flaschka, W. Meyer and T. Ratiu Editors. (1990).

[4] Y. Li and D.W. McLaughlin, Homoclinic Orbits and Chaos in Discretized Perturbed NLS Systems. I. Homoclinic Orbits. *J. Nonlinear Science* **7** (1997) 211-269.

[5] Y. Li and D.W. McLaughlin, Morse and Mel'nikov Functions for NLS Pde's Discretized Perturbed NLS Systems. I. Homoclinic Orbits. *Comm. Math. Phys.* **612** (1994) 175-214.

[6] Ablowitz, M.J., Herbst, B. and Schober, C.M., Computational Chaos in the Nonlinear Schrödinger Equation without Homoclinic Crossings, *Physica A* **228** 1996.

[7] Y. Li, D.W. McLaughlin and J. Shatah, Persistent Homoclinic Orbits for Perturbed NLS Equation, Preprint, 1995.

[8] Ablowitz, M.J., Henderson, D., Hammack, J. and Schober, C.M., Modulated Periodic Stokes Waves in Deep Water, to be published *Physical Review Letters*, Jan. 2000.

[9] G.Haller and S. Wiggins, Multi-pulse jumping orbits and homoclinic trees in a modal truncation of the damped-forced NLS equation, *Physica D* **85** (1995) 311–347.